

Soft Matter

Accepted Manuscript



This is an *Accepted Manuscript*, which has been through the Royal Society of Chemistry peer review process and has been accepted for publication.

Accepted Manuscripts are published online shortly after acceptance, before technical editing, formatting and proof reading. Using this free service, authors can make their results available to the community, in citable form, before we publish the edited article. We will replace this *Accepted Manuscript* with the edited and formatted *Advance Article* as soon as it is available.

You can find more information about *Accepted Manuscripts* in the [Information for Authors](#).

Please note that technical editing may introduce minor changes to the text and/or graphics, which may alter content. The journal's standard [Terms & Conditions](#) and the [Ethical guidelines](#) still apply. In no event shall the Royal Society of Chemistry be held responsible for any errors or omissions in this *Accepted Manuscript* or any consequences arising from the use of any information it contains.

Cite this: DOI: 10.1039/c0xx00000x

www.rsc.org/xxxxxx

ARTICLE TYPE

Nanostructures in Superhydrophobic Ti6Al4V Hierarchical Surfaces Control Wetting State Transitions

Yizhou Shen, Jie Tao*, Haijun Tao, Shanlong Chen, Lei Pan and Tao Wang

Received (in XXX, XXX) Xth XXXXXXXXX 20XX, Accepted Xth XXXXXXXXX 20XX

DOI: 10.1039/b000000x

This paper mainly reports the wetting state of liquid droplets on Ti6Al4V micro-nanoscale hierarchical structured hydrophobic surface. In this work, the detailed action mechanism of the secondary nanostructure in the hierarchical structure on the wetting-state transition (from the Wenzel state to the Cassie state) was revealed and discussed. The variation of micro-morphology of the sample surface was observed using a field emission scanning electron microscope (FE-SEM). Furthermore, the apparent contact angle and sliding angle of the droplets on the surfaces were measured via a contact angle measurement instrument. The theoretical and experimental results indicated that the one-dimensional nanowire structure, which was planted on the microstructure surface by the hydrothermal method, effectively changed the wetting state of liquid droplets on the surface from the Wenzel state to the Cassie state owing to its good size synergies with microscale structure. This process not only increased the apparent contact angle of liquid droplets on the solid surface (to 161°), but also decreased the sliding angle significantly (to 3°) and contact angle hysteresis (to $\sim 2^\circ$), demonstrating the robust non-wetting property.

Introduction

Surface wetting is one of the important properties of a solid surface and one of the most common interfacial phenomena such as a droplet of morning dew on a lotus leaf and a mercury droplet on a glass surface (in contrast to a water droplet that spread out on a glass surface).¹⁻³ In general, the contact angle θ is used to characterize the wetting state on a solid surface. When $\theta < 90^\circ$, the liquid can partially wet the solid and completely wet in $\theta = 0^\circ$, and the solid surface is called a hydrophilic surface or superhydrophilic surface. When $\theta > 90^\circ$, the liquid cannot wet the solid, and the solid surface is called a hydrophobic surface. Actually, some special surfaces have a contact angle of $> 150^\circ$ and the droplets on these surfaces can very easily roll away (contact angle hysteresis $< 10^\circ$), being defined as superhydrophobic surfaces.^{4,5}

Superhydrophobic surfaces have attracted much attention from researchers in the world because of their great potential in different applications, particularly in fields such as waterproofing,⁶ self-cleaning,^{7,8} anti-corrosion,⁹ drag-reducing,¹⁰ and anti-frosting.^{11,12} Since the published studies on hierarchical superhydrophobic surfaces and animal and plant surfaces by Japanese and German scientists in the 1990s,^{13,14} extensive progress has been made in this field. Researchers applied micro-/nanoprepation techniques to construct superhydrophobic surfaces similar to lotus leaves, butterfly wings, and water strider legs on metal or glass substrate,^{15,16} achieving the perfect unity of microstructure and property.

The main factors affecting the wettability of a solid surface are

chemical component (or surface free energy) and geometrical microstructure (or surface roughness).¹⁷ On a smooth surface, the contact angle of a liquid droplet can be increased to 120° by lowering the surface free energy. Adding the construction of a micro-nanostructure, the contact angle of droplets can be increased to 150° or beyond.¹⁸ Currently, processes such as micromachining,¹⁹ laser or plasma etching,^{20,21} physical or chemical vapor deposition,^{22,23} sol-gel,²⁴ phase separation²⁵, electrostatic spinning,²⁶ and spraying²⁷ have been developed to successfully prepare and use superhydrophobic surfaces in different application fields. Qian and Shen used dislocation etching to build nanostructured surfaces on aluminum, copper, and zinc substrates and obtain superhydrophobicity after fluorination modification.²⁸ Zhang and co-workers combined chemical and electrochemical corrosion methods to construct a micro-nanocomposite hierarchical structure on aluminum alloy surface, which also showed a high superhydrophobicity after fluorination modification.²⁹ Caihong Xu's group utilized a simple and inexpensive solidification-induced phase-separation method to fabricate highly transparent and durable superhydrophobic coatings ($\theta \approx 155^\circ$). Moreover, the nanoscale surface roughness of the coatings can be easily adjusted via changing the process parameters.³⁰ Ishizaki *et al.* developed a facile and time-saving method of creating a superhydrophobic surface on a magnesium alloy by a simple immersion process at room temperature. The film was covered with fluoroalkylsilane molecules, resulting in a robust superhydrophobicity (contact angle of more than 150°).³¹

As above, current research efforts about superhydrophobic surfaces are mainly focused on the construction of micro-/nanostructures and the evaluation of their properties. The action

mechanism of structure on hydrophobicity and the dynamic behavior of liquid droplets on the surfaces are still not clear. Although the hierarchical structure of surfaces was introduced in the 1990s, no substantial progress has been made in understanding the mechanism of action of the hierarchical structure, particularly the secondary nanostructure, on the non-wetting performance. Although the Wenzel and Cassie models play a significant role in the theoretical studies on wettability of the non-ideal rough surfaces, further studies are needed to understand the transition mechanism from the Wenzel wetting state of the primary rough structured hydrophobic surfaces to the Cassie wetting state of the hierarchical structured superhydrophobic surfaces.

As mentioned above, a full understanding of the action mechanism of a hierarchical structure on the non-wetting performance and the dynamic behavior of droplets on the surfaces is of great importance for the development of superhydrophobic techniques. Currently, Ti6Al4V alloy has been widely used to manufacture the leading edges of the wing or engine inlet in aircraft fields owing to the excellent mechanical properties. When the aircraft flies in some cold regions, ice accretion will occur on the surface of the aircraft, especially on the leading edge surface. We believe that the superhydrophobic Ti6Al4V surface can effectively reduce the ice build-up, and its anti-icing potential has been also reported in our previous article.³² Thus, we utilized a combination of sand blasting and hydrothermal method to rapidly construct the micro-nanoscale hierarchical structures on a Ti6Al4V surface in this work, and followed by fluorination modification, thus forming a hydrophobic surface. The mechanism of action of the hierarchical structure on the wetting state of liquid droplets, particularly the effect of the secondary nanostructure on the wetting-state transition of droplets on the surfaces from the Wenzel state to the Cassie state, was investigated.

Experimental section

Materials

The following materials were used: Ti6Al4V titanium alloy (composition (wt-%): $\leq 0.3\%$ Fe, $\leq 0.1\%$ C, $\leq 0.05\%$ N, $\leq 0.015\%$ H, $\leq 0.2\%$ O, 5.5~6.8% Al, 3.5~4.5% V, and the rest is Ti) with a size of 10 mm \times 10 mm \times 1 mm (Baoji Titanium Industry Co., Ltd., China); 1*H*,1*H*,2*H*,2*H*-perfluorodecyltrimethoxysilane (FAS-17) (Tokyo Chemical Industry Co., Ltd., Japan); other reagents: sodium hydroxide, hydrochloric acid, ethanol, and acetone (Sinopharm Chemical Reagent Co., Ltd., China), these chemicals were analytical grade.

Experimental Procedure

Sample pretreatment: The sample surfaces were polished with metallographic sandpaper (No. 0-6) and then cleaned ultrasonically in acetone, ethanol, and deionized water for 10 min sequentially and dried. **Sandblasting:** Sand blasting of the polished samples was conducted using aluminum oxide (60 mesh, 150 mesh, and 300 mesh) at 0.5 MPa for 10 s. The samples were ultrasonically cleaned with acetone, ethanol, and deionized water sequentially for 10 min and then dried for further use. **Hydrothermal treatment:** The sand blasted samples were placed in

an autoclave with 30 mL of 1 M NaOH solution in a 220 °C oven and reacted for different times (1 h, 2 h, 4 h, 6 h, 8 h, and 12 h). After cooling down to room temperature, the samples were removed from the autoclave and immersed in 1 M HCl solution for 30 min. Next, the sample surfaces were rinsed with deionized water. Finally, the samples were placed in a muffle furnace (heating rate was 2 °C s⁻¹) and heated at 500 °C for 3 h to produce TiO₂ nanowires. **Fluorination modification:** The hydrothermally treated samples were immersed in 1 wt% FAS-17 ethanol solution for 24 h and then dried in a 120 °C oven for 2 h to obtain the final samples.

Characterizations

The surface morphologies of the samples were observed using a field emission scanning electron microscope (FE-SEM; Hitachi S4800, Japan). An infrared radiation (FT-IR) spectrum was acquired to characterize the surface groups of samples with an infrared spectrometer (Nicolet Nexus 670, USA). The apparent contact angle (APCA), the sliding angle (SA) and contact angle hysteresis (CAH) of a 4 μ L water droplet on these surfaces were measured by a contact angle analyzer (Kruss DSA100, Germany). APCA could be directly obtained by the contact angle analyzer. CAH was the difference of advancing contact angle and receding contact angle. Advancing contact angle was recorded by the computer, when the contact area of the droplet with surface changed owing to expansion of droplet. If the contact area decreased via shrinking the droplet, receding contact angle could be recorded. The average value of three measurements was determined. In order to ensure that the 4 μ L water droplet successfully dripped on the surfaces, we chose the ultrafine syringe needle with the inner diameter of only 0.03 mm, which was also hydrophobized with FAS-17.

Results and discussion

Preparation of the hierarchical structure superhydrophobic surfaces

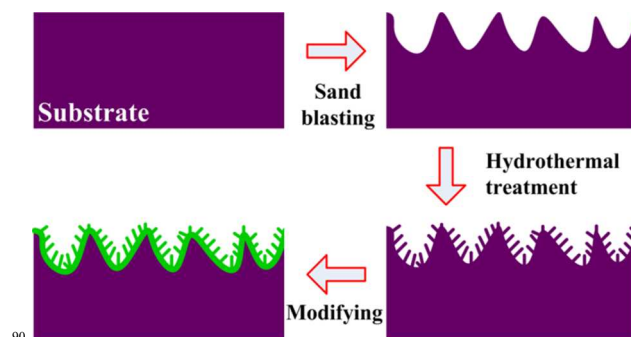


Fig. 1. Schematic diagram of the construction process of micro-nanoscale hierarchical structures and fluorination modification.

Preparation of superhydrophobic surfaces is based on the combination of micro-nanostructure (roughness) and surface chemical composition.³³ Roughness is a key element to prepare the superhydrophobic surfaces. In this work, it can be divided into two parts of building micro-nanoscale hierarchical structures and fluorination modification, as shown in Figure 1. The primary microscale rough structure was constructed by a traditional sand

blasting method. High-speed hard aluminum oxide particles continuously impacted the titanium alloy surface, causing erosion and forming uneven rough structured surfaces like microhills.³⁴ The hydrothermal treatment of the sample led to the growth of one-dimensional (1D) TiO₂ nanowires on the surface of the microscale rough structure. This process significantly increased the specific surface area of the sample, resulting in the increase of the grafted area with the fluorine-containing low-surface-energy groups.³⁵

Because of the extremely low surface free energy of FAS-17, it is widely used to modify rough structures for making the solid surface hydrophobic.^{36,37} The grafting process of FAS-17 hydrophobic groups is shown in Figure 2. Hydrolysis of the Si-OR groups of FAS-17 in ethanol generated Si-OH groups, which formed covalent bonds with the TiO₂ molecules on the solid surface through condensation reactions. Furthermore, the FAS-17 molecules on the surface were also connected to each other by covalent bonds formed through intermolecular condensation reactions.

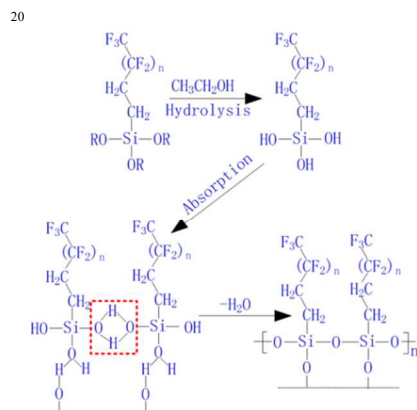


Fig. 2. Grafting process of FAS-17 hydrophobic groups with solid surface.

Figure 3 shows the FT-IR spectrum of the surface hydrophobic groups. After fluorination modification with FAS-17, the characteristic absorption peak of the CF₂ bond appeared ~1243.32 cm⁻¹. And the characteristic absorption peak of the C-F bond was ~1161.32 cm⁻¹ while that for the C-H bond was ~2935.89–2962.28 cm⁻¹.³⁸ According to this spectrum, the FAS-17 hydrophobic groups were successfully grafted to the microscale hierarchical surface after the fluorination modification.

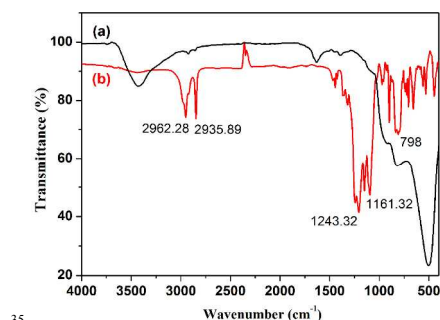


Fig. 3. FT-IR spectrum of surface hydrophobic groups; (a) before fluorination modification, (b) after fluorination modification.

Wenzel wetting state of primary microscale surfaces

Figure 4 shows the morphologies of the primary sand blasted Ti6Al4V surface. The sand blasting with 60-mesh aluminum oxide formed a large-size concave-convex structure (~60 μm). In comparison, 150-mesh aluminum oxide led to relatively even concave-convex structure (~35 μm). The use of 300-mesh aluminum oxide formed an even finer structure with a smooth overall topography. Subsequently, the fluorination modification of the sand blasted microscale structure with FAS-17 just resulted in a hydrophobic surface. The results of apparent contact angle measurements on these surfaces are shown in Figure 4, inset. We could conclude that the sand blasted sample with 150-mesh aluminum oxide followed by fluorination modification had the largest contact angle of liquid droplets (~135°) among these microscale structure surfaces.

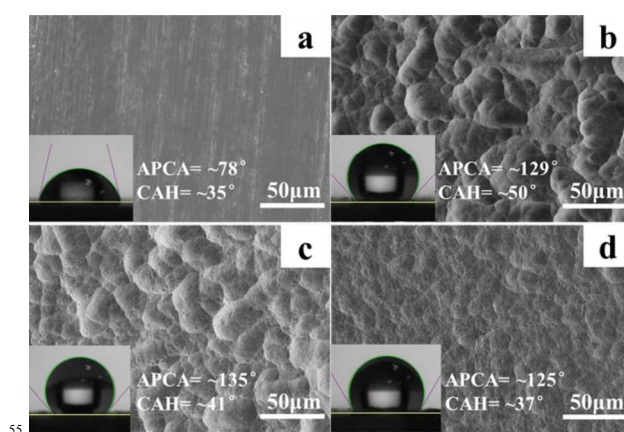


Fig. 4. FE-SEM images of the sand blasted microstructure with the fluorination modification using FAS-17; (a) Smooth substrate, (b) with 60 mesh aluminum oxide, (c) with 150 mesh aluminum oxide, (d) with 300 mesh aluminum oxide.

For the hydrophobic surfaces of the primary microscale (20–100 μm) structures, the contact angle of the liquid droplets on solid surface followed the Wenzel wetting model,³⁹ as shown in Figure 5. The actual contact angle of the droplet on a rough structure surface is unmeasurable. The contact angle obtained from the experiment is the apparent contact angle θ^* . The apparent contact angle does not fit the Young's equation:

$$\gamma_{LV} \cos \theta = \gamma_{SV} - \gamma_S \quad (1)$$

According to the Wenzel model the ideal contact angle θ by the true angle θ^* :

$$\cos \theta^* = r \cos \theta \quad (2)$$

Where, r is defined as the roughness factor, *i.e.*, the ratio of actual solid/liquid interfacial contact area to the apparent solid/liquid interfacial contact area ($r \geq 1$). θ is the Young's contact angle, *i.e.*, the contact angle of the liquid droplets on the fluorination-modified Ti6Al4V substrate in this paper. The apparent contact angle θ^* increases with the increase in the roughness factor r . Geometrically analyzing, the existence of a microscale (20–100 μm) structure surface certainly results in a larger actual solid/liquid interfacial contact area than the apparent contact area, leading to a higher apparent contact angle θ^* of the liquid droplets

comparing to the Young's contact angle θ . The surface roughness of the sand blasted structure surface with 60-mesh aluminum oxide increased with slightly reducing in the roughness factor r ($r \approx 1.07$, see Supporting Information), compared with that ($r \approx 1.09$) of the sand blasted structure surface with 150-mesh aluminum oxide. Thus, for the liquid droplets in the Wenzel wetting state, the increase in roughness factor r significantly improved the hydrophobicity.

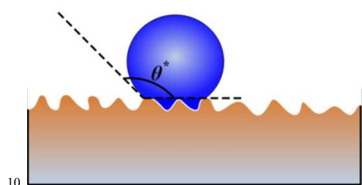


Fig. 5. Wenzel wetting model.

Transition from the Wenzel Wetting State to the Cassie Wetting State

To further increase the roughness factor r , a layer of 1D TiO₂ nanowires was planted (through the hydrothermal process) on the microstructure surface formed by sand blasting with 150-mesh aluminum oxide.⁴⁰ The morphological changes are shown in Figure 6. After the fluorination modification with FAS-17, the apparent contact angle and contact angle hysteresis changes are shown in Figure 7c. With a short hydrothermal reaction time (1-2 h), the formed nanowires were relatively short and small, the apparent contact angle of the droplets on the surfaces increased slowly from approximately 135° to 138°. When the hydrothermal reaction time reached 4 h, the nanowire length increased with relatively even distribution, and the endings gradually gathered. As the hydrothermal reaction time was even longer (8 h), the nanowire length further increased, and more dense distribution was observed on the surfaces of microscale structures. Meanwhile, the apparent contact angle of droplets on the surfaces also obtained a very obvious increase to 161°. We also found that the apparent contact angle nearly remained unchanged, when the hydrothermal reaction time was even longer.

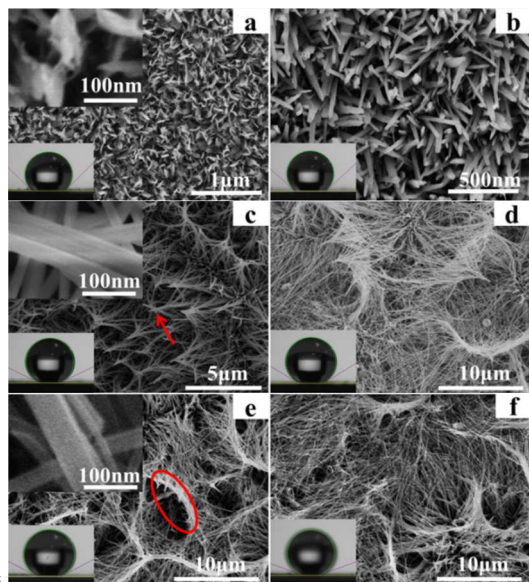


Fig. 6 Effect of hydrothermal process time on the secondary nanostructures (a) 1 h, (b) 2 h, (c) 4 h, (d) 6 h, (e) 8 h, and (f) 12 h.

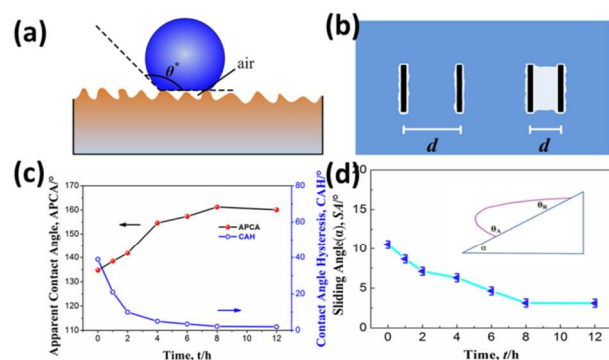


Fig. 7 (a) Cassie wetting model, (b) Nanostructure surface air layer illustration, (c) Apparent contact angle and contact angle hysteresis, (d) Variation in sliding angle with the extension of hydrothermal reaction time.

In this time, the clear explanations of the effect of secondary nanostructures on the apparent con-tact angle are necessary. Why does the apparent contact angle increase significantly with the addition of secondary nanowire structures to microscale textures? The micro-nanoscale hierarchical structure is also one type of rough surface. We can continue to use the Wenzel equation to reveal the relationship between the apparent contact angle and Young's contact angle. However, owing to the existence of nanowire structures on the microscale structure surface, the roughness factor r is very large, even an infinite value, causing a very large apparent contact angle. Strictly speaking, the Wenzel equation is not applicable in this case.

Based on the Wenzel and Cassie equations, through the simulation of a rough surface, Dettre and Johnson drew a conclusion that there was a critical value of the roughness factor of a solid surface for the transition of wetting state.⁴¹ At this critical value, the liquid droplets on the solid surface change from the Wenzel wetting state to the Cassie wetting state, as shown in Figure 7a. For one hydrophobic nanowire, large amounts of hydrophobic groups are present on the surface, and repel the adjacent hydrogen bonds from water. Thus, water is removed from the surface, and a thin layer of air is generated near the nanowire. This is a metastable state. When the spacing distance of each two nanowires is smaller than a certain value d' , the thin air layers would attract each other to form a larger continuous air layer, as shown in Figure 7b. d' can be calculated via the formula:

$$d' \approx \frac{2\gamma}{n_l |\mu_l - \mu_g|} \quad (3)$$

Where γ is the surface tension of liquid; $\mu_l - \mu_g$ is the chemical potential difference of liquid and gas; n_l is the density of liquid molecules. For the water at standard conditions of 1 atm and $T=298$ K, n_l is about 0.055 mol cm⁻³; γ is 72 mJ m⁻²; and $\mu_l - \mu_g$ is -1.8 J mol⁻¹.⁴² Thus, d' is calculated approximately 100 nm.

Combined with the microscale structure, a huge amount of air can be trapped underneath the liquid droplets and gradually form a stable Cassie wetting state, resulting in the water droplets being suspended on the surface. According to the Cassie equation:

$$\cos \theta^* = f_1 \cos \theta_1 + f_2 \cos \theta_2 \quad (4)$$

In the equation, θ_1 and θ_2 represent the Young's contact angles of the liquid droplet on the solid and air; f_1 and f_2 are the apparent contact area fractions of the liquid droplet on the solid and air, and $f_1 + f_2 = 1$. Because the Young's contact angle of liquid droplet on air is 180° , equation (4) becomes:

$$\cos \theta^* = f_1 \cos \theta_1 + f_2 - 1 \quad (5)$$

Thus, the apparent contact angle θ^* depends on the apparent contact area fractions of the liquid droplet on the solid f_1 . With a short hydrothermal reaction time (1-2 h), the formed nanowires were relatively short and small, leading to the surface wetting state in the transition state between the Wenzel wetting state and the Cassie wetting state. As the hydrothermal reaction time was prolonged, the generated nanowire length further increased, and more densely distributed. Furthermore, the spacing distance between the nanowires with each other was far less than 100 nm, forming a larger continuous air layer. Thus, with the addition of secondary nanowire structures to microscale textures, the wetting regime of the liquid droplets on the solid surface successfully changed from the Wenzel wetting state to the Cassie wetting state.

When the hydrothermal reaction time is 8 h, the generated secondary nanowires and microscale structure can trap a large amount of air (f_1 is very small, $\approx 10\%$), resulting in an apparent contact angle of 161° . Moreover, the specially entwined nanowire structure formed through the hydrothermal process favors the air flow underneath the droplets. The "grooming" of this "ridge"-like structure leads to the easy sliding of the liquid droplets and shows outstanding hydrophobic function (the sliding angle decreased to $\sim 3^\circ$, as shown in Figure 7d). Thus, the construction of 1D secondary nanowire structure on the microscale structure surface through the hydrothermal process can effectively change the wetting state of liquid droplet on the rough surface from the Wenzel state to the Cassie state. This process not only increased the apparent contact angle of liquid droplets on the solid surface (to 161°), but also decreased the sliding angle significantly (to 3°) and contact angle hysteresis (to $\sim 2^\circ$), demonstrating the robust non-wetting property.

Conclusions

On the Ti6Al4V hydrophobic surface with a micro-nanoscale hierarchical structure, large amounts of hydrophobic groups accumulated near the secondary nanowires, and repelled the adjacent hydrogen bonds from water, thus removing water from the surface. Next, a thin layer of air was formed around the nanostructure. This was a metastable state. When the spacing distance of the nanostructure was smaller than a certain value d' , the thin air layers would attract each other to form a larger continuous air layer. Combined with a certain size of microscale structure, this could hold liquid with a certain volume on the rough structure surface, achieving the transition from the Wenzel wetting state to the Cassie wetting state. The contact angle of a liquid droplet increased from 134.75° to 161° , the sliding angle decreased from 12° to 3° , and the contact angle hysteresis decreased to $\sim 2^\circ$.

Acknowledgements

The authors gratefully acknowledge the financial support of the National Science Foundation of China (No. 51475231, No.

51202112), A Project Funded by the Priority Academic Program Development of Jiangsu Higher Education Institutions, the Jiangsu Innovation Program for Graduate Education (KYLX_0261) and the Fundamental Research Funds for the Central Universities.

Notes and references

* Corresponding author: Professor Jie Tao

Tel/Fax.: +86 25 5211 2911.

E-mail address: taojie@nuaa.edu.cn.

College of Material Science and Technology, Nanjing University of Aeronautics and Astronautics, Nanjing 210016, P. R. China

- 1 F. Zhou and W. T. S. Huck, *Chem. Commun.*, 2005, 5999-6001.
- 2 G. S. Watson, M. Gellender and J. A. Watson, *Biofouling*, 2014, **30**, 427-434.
- 3 K. Liu, X. Yao and L. Jiang, *Chem. Soc. Rev.*, 2010, **39**, 3240-3255.
- 4 B. N. Sahoo and B. Kandasubramanian, *RSC Adv.*, **4**, 22053-22093.
- 5 H. B. Eral, D. J. C. M. Manette and J. M. Oh, *Colloid Polym. Sci.*, 2013, **291**, 247-260.
- 6 M. Ma and R. M. Hill, *Curr. Opin. Colloid In.*, 2006, **11**, 193-202.
- 7 A. Nakajima, K. Hashimoto and T. Watanabe, *Langmuir*, 2000, **16**, 7044-7047.
- 8 Y. Lai, Y. Tang, J. Gong, D. Gong, L. Chi, C. Lin and Z. Chen, *J. Mater. Chem.*, 2012, **22**, 7420-7426.
- 9 Y. Chen, S. Chen, F. Yu, W. Sun, H. Zhu and Y. Yin, *Surf. Interface Anal.*, 2009, **41**, 872-877.
- 10 R. J. Daniello, N. E. Waterhouse and J. P. Rothstein, *Phys. Fluid*, 2009, **21**, 085103: <http://dx.doi.org/10.1063/1.3207885>.
- 11 L. B. Boinovich and A. M. Emelyanenko, *Mendeleev Commun.*, 2013, **23**, 3-10.
- 12 M. Ruan, W. Li, B. Wang, B. Deng, F. Ma and Z. Yu, *Langmuir*, 2013, **29**, 8482-8491.
- 13 T. Onda, S. Shibuichi, N. Satoh and K. Tsujii, *Langmuir*, 1996, **12**, 2125-2127.
- 14 W. Barthlot and C. Neinhuis, *Planta*, 1997, **202**, 1-8.
- 15 T. Darmanin and F. Guittard, *J. Mater. Chem.*, 2014, **2**, 16319-16359.
- 16 M. Liu, S. Wang, Z. Wei, Y. Song and L. Jiang, *Adv. Mater.*, 2009, **21**, 665-669.
- 17 Y. K. Lai, J. Y. Huang, J. J. Gong, Y. X. Huang, C. L. Wang, Z. Chen and C. J. Lin, *J. Electrochem. Soc.*, 2009, **156**, 480-484.
- 18 Y. Shen, H. Tao, S. Chen, Y. Xie, T. Zhou, T. Wang and J. Tao, *Appl. Surf. Sci.*, 2014, **321**, 469-474.
- 19 X. T. Zhang, J. Liang, B. X. Liu and Z. J. Peng, *Colloid. Surface A.*, 2014, **454**, 113-118.
- 20 D. Kontziampasis, G. Boulousis, A. Smyrnakis, K. Ellinas, A. Tseripi and E. Gogolides, *Microelectron. Eng.* 2014, **121**, 33-38.
- 21 P. Roach, N. J. Shirtcliffe and M. I. Newton, *Soft Mater*, 2008, **4**, 224-240.
- 22 J. Wang, X. Song, R. Li, J. P. Shen, G. C. Yang and H. Huang, *Appl. Surf. Sci.*, 2012, **258**, 9782-9785.
- 23 A. Hozumi, B. Kim and T. J. McCarthy, *Langmuir*, 2009, **25**, 6834-6840.
- 24 J. Liu, W. Huang, Y. Xing, R. Li and J. Dai, *J. Sol-gel Sci. Techn.*, 2011, **58**, 18-23.
- 25 C. Lopresti, M. Massignani, C. Fernyhough, A. Blanazs, A. J. Ryan, J. Madsen, N. J. Warren, S. P. Armes, A. L. Lewis, S. Chirasatitsin, A. J. Engler and G. Battaglia, *ACS Nano*, 2011, **5**, 1775-1784.
- 26 M. L. Ma, Y. Mao, M. Gupta, K. K. Gleason and G. C. Rutledge, *Macromolecules*, 2005, **38**, 9742-9748.
- 27 H. Ogihara, J. Xie, J. Okagaki and T. Saji, *Langmuir*, 2012, **28**, 4605-4608.
- 28 B. T. Qian and Z. Q. Shen, *Langmuir*, 2005, **21**, 9007-9009.
- 29 Z. Wang, Q. Li, Z. She, F. Chen, L. Li, X. Zhang and P. Zhang, *Appl. Surf. Sci.*, 2013, **271**, 182-192.
- 30 D. Wang, Z. Zhang, Y. Li and C. Xu, *ACS Appl. Mater. Inter.*, 2014, **6**, 10014-10021.
- 31 T. Ishizaki and N. Saito, *Langmuir*, 2010, **26**, 9749-9755.

- 32 Y. Shen, H. Tao, S. Chen, L. Zhu, T. Wang and J. Tao, *RSC. Adv.*, 2015, **5**, 1666-1672.
- 33 J. Bico, C. Marzolin and D. Quéré, *Europhys. Lett.*, 1999, **47**, 220-226.
- 34 M. K. Kang, S. K. Moon, J. S. Kwon, K. M. Kim and K. N. Kim, *Mater. Res. Bull.*, 2012, **47**, 2952-2955.
- 5 35 J. Li, W. Wan, H. Zhou, J. Li and D. Xu, *Chem. Comm.*, 2011, **47**, 3439-3441.
- 36 M. He, Q. Zhang, X. Zeng, D. Cui, J. Chen, H. Li, J. Wang and Y. Song, *Adv. Mater.*, 2013, **25**, 2291-2295.
- 10 37 N. Saleema, D. K. Sarkar, D. Gallant, R. W. Paynter and X. G. Chen, *ACS Appl. Mater. Inter.*, 2011, **3**, 4775-4781.
- 38 D. Schondelmaier, S. Cramm, R. Klingeler, J. Morenzin, C. Zilkens and W. Eberhardt, *Langmuir*, 2002, **18**, 6242-6245.
- 39 E. Bormashenko, R. Pogreb, T. Stein, G. Whyman, M. Erlich, A. Musin, V. Machavariani and D. Aurbach, *Phys. Chem. Chem. Phys.*, 2008, **10**, 4056-4061.
- 15 40 J. M. Wu, H. C. Shih and W. T. Wu, *Nanotechnology*, 2006, **17**, 105 doi: 10.1088/0957-4484/17/1/017.
- 41 J. R. E. Johnson and R. H. Dettre, *Adv. Chem. Ser.*, 1963, **43**, 112.
- 20 42 K. Lum, D. Chandler and J. D. Weeks, *J. Phys. Chem. B*, 1999, **103**, 4570-4577.

TOC

